ACS APPLIED MATERIALS & INTERFACES

Research Article

Cite This: ACS Appl. Mater. Interfaces 2018, 10, 13660−13668

www.acsami.org

Redefinition of Crystal Structure and Bi^{3+} Yellow Luminescence with Strong Near-Ultraviolet Excitation in $La_3BWO_9:Bi^{3+}$ Phosphor for White Light-Emitting Diodes

Jin Han,[†] Fengjuan Pan,[‡] Maxim S. Molokeev,[§,∥,⊥] Junfeng Dai,[†] Mingying Peng,*[,†] Weijie Zhou,[#] and Jing Wang[#]

[†]State Key Laboratory of Luminescent Materials and Devices, Guangdong Engineering Technology Research and Development Center of Special Optical Fiber Materials and Devices, and Guangdong Provincial Key Laboratory of Fiber Laser Materials and Applied Techniques, School of Materials Science and Engineering, South China University of Technology, Guangzhou 510641, China

[‡]College of Chemistry and Molecular Engineering, Peking University, Beijing 100871, China

[§]Laboratory of Crystal Physics, Kirensky Institute of Physics, Federal Research Center KSC SB RAS, Krasnoyarsk 660036, Russia

[∥]Department of Physics, Far Eastern State Transport University, Khabarovsk 680021, Russia

[⊥]Siberian Federal University, Krasnoyarsk 660079, Russia

[#]School of Chemistry, Sun Yat-Sen University, Guangzhou 510275, China

ABSTRACT: Bi^{3+}-activated photonic materials have received increased interest recently because they can be excited effectively with near-ultraviolet (NUV) but not visible light, thereby avoiding the reabsorption among phosphors, which cannot be solved intrinsically by traditional rare earth (e.g., Eu^{2+}, Ce^{3+}) phosphors. Such unique property suggests their potential application in NUV chip-based WLEDs. However, few Bi^{3+} phosphors exhibit strong excitation peak in NUV, though the excitation tail of some can extend to NUV. Herein, we report a novel yellow-emitting $La_3BWO_9:Bi^{3+}$ (LBW:Bi^{3+}) phosphor with strong NUV excitation. The photoluminescence (PL) spectroscopy analysis indicates that there are two Bi^{3+} luminescent centers in LBW:Bi^{3+} phosphor, which is clearly in contradiction with the established hexagonal structure of La_3BWO_9 with $P6_3$ space group because only one La site in this structure can accommodate Bi^{3+} ions. Combining the luminescent properties of Bi^{3+} with Rietveld refinement, La_3BWO_9 was redefined as a trigonal structure with the lower space group of $P3$ in which there are two independent crystallographic La sites. In addition, the rationalization of $P3$ space group was further confirmed by the finding of the reflection (0001) according to the extinction rule. Therefore, the PL behavior of Bi^{3+} can act as a complementary tool to determine the real crystal structure especially when it is hard to distinguish by conventional X-ray diffraction techniques.

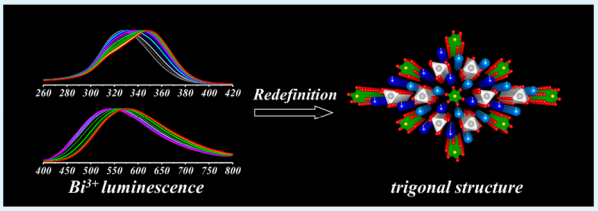

KEYWORDS: *borotungstates, yellow phosphor, Bi^{3+} luminescence, X-ray diffraction, crystal structure, WLEDs*

1. INTRODUCTION

In the last few decades, tremendous human and material resources have been invested in developing rare earth (e.g., Eu^{2+}) and non-rare earth (e.g., Mn^{2+}) related luminescent materials for phosphor-converted white light-emitting diodes (pc-WLEDs), while the majority of products have failed to meet the requirements of practical application owing to the intrinsic problems of these dopants such as unavoidable visible light reabsorption and weak absorption in the near-ultraviolet (NUV) region.[1−4] A competitive phosphor must have strong absorption within the emission spectrum of the LED chip, excellent chemical and thermal stability, high quantum yield, fast decay time, low cost, etc. Such stringent requirements set up barriers on host materials and activator ions, thus narrowing the number of accessible phosphors for pc-WLEDs.[5−8]

Commercially available WLEDs are fabricated by combining Ce^{3+}-doped yttrium aluminum garnet yellow phosphor with blue InGaN LED chip. However, the quality of white light has been greatly restricted by poor color rendering index (typically lower than 80) and high correlated color temperature (typically within 4000−8000 K). This is due to the poor contribution of YAG:Ce^{3+} in the red spectral range.[9−11] Another alternative approach involves combining blue, green, and red phosphors with a NUV LED chip (λ = 350−410 nm). The roles of green and red phosphors in the scheme can be replaced by yellow phosphors because yellow light can be realized by blending green and red light. As a result, yellow-emitting phosphors are preferred to be used together with blue-emitting phosphors to obtain white light emission if a high color rendering index is not required.

Received: January 15, 2018
Accepted: April 2, 2018
Published: April 2, 2018

DOI: 10.1021/acsami.8b00808
ACS Appl. Mater. Interfaces 2018, 10, 13660−13668

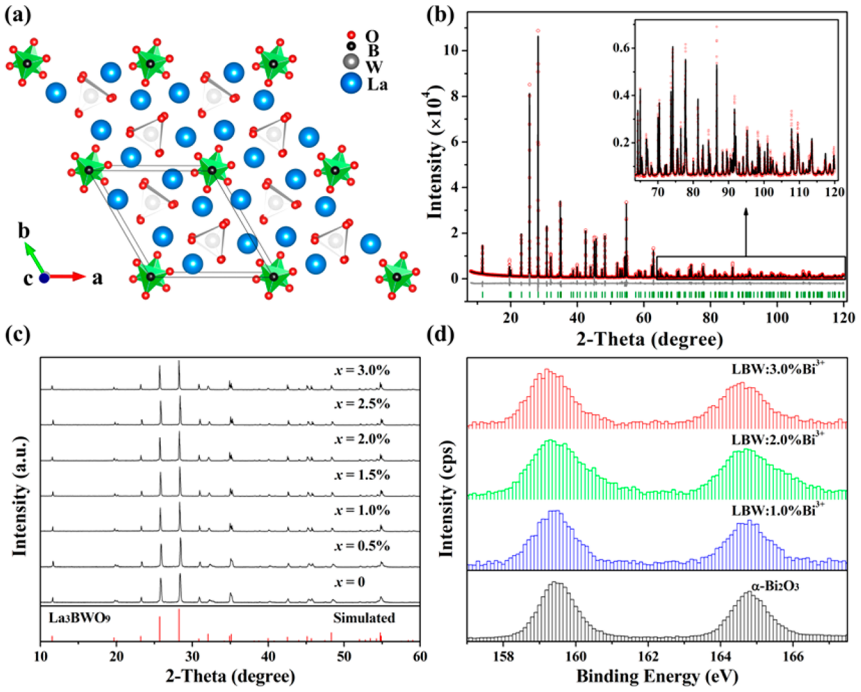

Figure 1. (a) Hexagonal structure of La_3BWO_9. (b) Observed (red dots) and calculated (black solid line) XRD patterns as well as difference profile (gray solid line) of Rietveld refinement for $La_{2.91}Bi_{0.09}BWO_9$ in $P6_3$ space group; the green ticks mark the Bragg reflection positions. (c) XRD patterns of La_3BWO_9:xBi^{3+} samples along with the simulated standard patterns of La_3BWO_9. (d) XPS spectra of La_3BWO_9:xBi^{3+} sample and α-Bi_2O_3 reference.

The types of luminescent centers for yellow phosphors can be divided into rare earth and non-rare earth. The typical rare earth ions which can emit yellow light are Eu^{2+} and Ce^{3+}. Eu^{2+} and Ce^{3+} have been proven as broadband activators (fwhm >70 nm) because their allowed 5d → 4f transitions are flexible to local crystal field surroundings.[12] Many rare earth-activated yellow phosphors were discovered over the last few decades, for example Sr_3SiO_5:Eu^{2+},[13] Li_2SrSiO_4:Eu^{2+},[14] $Sr_8ZnSc(PO_4)_7$:Eu^{2+},[15] $SrAlSi_4N_7$:Ce^{3+},[16] and $La_3BaSi_5N_9O_2$:Ce^{3+}.[17] Nevertheless, some phosphors doped with Eu^{2+} and Ce^{3+} exhibit strong absorption bands which lie in the blue-green region, and therefore, low luminous efficiency arises owing to the reabsorption among phosphors. In this case, non-rare earth, i.e. Bi^{3+}, doped yellow phosphors would be ranking. As Eu^{2+} and Ce^{3+} ions, Bi^{3+} can emit various color light from ultraviolet to red in different host materials, and its luminescence strongly depends on the surrounding crystal field and coordination environment in the host lattice.[18,19] Accordingly, the PL behavior of Bi^{3+} can serve as a good indicator to evaluate the crystal structure for a given host compound. Unfortunately, few studies have been involved in Bi^{3+} phosphors. As previously reported by Peng et al., Bi^{3+} doped materials have characteristic excitation in NUV rather than in the visible region, for instance $ZnWO_4$:Bi^{3+} and $ScVO_4$:Bi^{3+}, revealing that they can avoid the problems traditional rare earth phosphors have encountered.[20,21]

Interest in rare earth-based borotungstates Ln_3BWO_9 (Ln = La, Pr, Nd, Sm−Ho) has remained high for years because of their potential for use as multifunctional optical materials.[22−24] Originally, the crystal structures of these compounds were defined as hexagonal with $P6_3$ space group by single-crystal X-ray diffraction.[25,26] There are single sites occupied by BO_3^{3-}, WO_6^{6-}, and Ln^{3+} ions in the lattice. Inspired by these, we selected La_3BWO_9 as the host compound to develop a yellow-emitting La_3BWO_9:Bi^{3+} (LBW:Bi^{3+}) phosphor with strong NUV excitation. The PL spectroscopy analysis shows that there are two Bi^{3+} luminescent centers in LBW:Bi^{3+} phosphor, which is inconsistent with the hexagonal structure of La_3BWO_9 with $P6_3$ space group because only one La site in this structure can be substituted by Bi^{3+} ions. A detailed analysis of the luminescent properties of Bi^{3+} was performed to correlate them with the local environment of Bi^{3+} in the host lattice. Combining the PL behavior of Bi^{3+} with Rietveld refinement, La_3BWO_9 was redefined as a trigonal crystal structure with $P3$ space group in which there are two independent crystallographic La sites.

2. EXPERIMENTAL SECTION

2.1. Sample Preparation. La_3BWO_9:Bi^{3+} (LBW:Bi^{3+}) powders were prepared by conventional high temperature solid state method. All chemicals, including H_3BO_3 (A. R.), WO_3 (A. R.), La_2O_3 (99.99%), and Bi_2O_3 (99.999%), were used as purchased without further purification. The target compounds were designed in the nominal chemical composition of $La_{3(1-x)}BWO_9$:$3xBi^{3+}$ ($0 \le x \le 3.0\%$) in consideration of the preferred occupancy of La sites by Bi^{3+} ions. The starting materials with stoichiometric molar ratios were ground and mixed thoroughly in an agate mortar. These mixtures were pretreated at 650 °C for 6 h, calcined at 1100 °C for 12 h in air atmosphere, and then slowly cooled to room temperature (RT). Final products were ground once again for subsequent tests.

2.2. Characterization. The phase purity of all samples was checked by X-ray diffraction (XRD) using a Bruker D8 ADVANCE powder diffractometer with Cu Kα radiation (λ = 1.54059 Å). High quality XRD data for Rietveld refinement were collected on a PANalytical Empyrean diffractometer in Bragg−Brentano geometry, using Cu Kα1 radiation source over a 2θ range from 5 to 120° with step width of 0.013°. Rietveld refinement was performed with TOPAS Academic 4.2 software.[27] The morphology of LBW:1.5%Bi^{3+} sample was observed by scanning electron microscopy (SEM, FEI Nova NanoSEM 430). The selected area electron diffraction (SAED)

DOI: 10.1021/acsami.8b00808
ACS Appl. Mater. Interfaces 2018, 10, 13660−13668

Table 1. Refined Structural Parameters for $La_{2.91}Bi_{0.09}BWO_9$ in $P6_3$ Space Group

atom	site	x	y	z	occ.	B_{iso} (Å^2)
W	2b	1/3	2/3	1/4	1	0.56(4)
La	6c	0.3636(1)	0.0854(1)	0.2213(5)	0.956(7)	0.74(4)
Bi	6c	0.3636(1)	0.0854(1)	0.2213(5)	0.044(7)	0.74(4)
B	2a	0	0	0.358(7)	1	2(1)
O1	6c	0.170(1)	0.047(2)	0.861(2)	1	2.0(2)
O2	6c	0.192(2)	0.483(2)	0.044(2)	1	2.0(2)
O3	6c	0.142(2)	0.517(2)	0.468(3)	1	2.0(2)
cell parameters	a = 8.84324 (5) Å, c = 5.57555 (4) Å, V = 377.609 (5) Å^3					
R factors	R_p = 5.55%, R_{wp} = 8.05%, R_B = 2.79%, χ^2 = 2.94					

pattern was taken on a JEOL JEM-2100F instrument. The valence state of Bi was identified by X-ray photoelectron spectroscopy (XPS) using a Kratos Axis Ultra DLD spectrometer equipped with a focused monochromatic Al Kα X-ray beam (1486.6 eV, 5 mA × 10 kV, ~5 × 10^{-9} Torr), and the binding energy was calibrated to the C 1s peak at 284.6 eV. The diffuse reflectance spectra (DRS) were collected on a Cary 5000 UV−vis−NIR spectrophotometer. The excitation and emission spectra as well as fluorescence decay curves at 10−500 K were recorded on an Edinburgh FLS920 steady-state and transient-state fluorescence spectrometer, which is equipped with a thermo-electric cooled red sensitive photomultiplier tube in the time-correlated single-photon counting mode. A 450 W xenon lamp, a 60 W μF900 flash lamp, and a 150 W nF900 flash lamp were used as the excitation light source. The temperature of the sample was adjusted by using a temperature controller (Tianjin Orient KOJI). The quantum efficiency (QE) was measured by using a Quantaurus-QY C11347-11 absolute PL quantum yield spectrometer.

3. RESULTS AND DISCUSSION

3.1. Crystal Structure of La_3BWO_9. In 1994, Gokhman et al. first solved the crystal structure of La_3BWO_9 by single-crystal X-ray diffraction.[28] La_3BWO_9 crystallizes in a hexagonal structure with the space group of $P6_3$ symmetry (no. 173). There are only one La site (6c), one B site (2a), and one W site (2b) in the hexagonal structure. As illustrated in Figure 1a, each W atom is surrounded by six O atoms, and its polyhedron, WO_6 octahedron, is a distorted trigonal prism sharing edges with three rare earth polyhedra. The rare earth ion La^{3+} resides in a noncentrosymmetric site which is 9-fold coordinated by nine O atoms (six O atoms from WO_6 groups and other three O atoms from BO_3 groups). The polyhedra of LaO_9 from different layers connect each other by sharing corners with BO_3 and WO_6 groups, forming the three-dimensional framework of La_3BWO_9. Considering charge and size match, only the La site in this structure can offer the great capacity to accept Bi^{3+} ions. The sample with the highest doping ratio of 3.0% was chosen for XRD structural refinement. Rietveld refinement was carried out using the $P6_3$ structure model defined by Gokhman et al.[28] There is only one La site in the structure and it is occupied by La^{3+} and Bi^{3+} ions. The occupancy was refined with linear restriction occ(La) + occ(Bi) = 1. Figure 1b presents the observed (red), calculated (black) XRD patterns of $La_{2.91}Bi_{0.09}BWO_9$, and difference profile (gray) of the structural refinement. The final reliability factors are converged to R_{wp} = 8.05% and R_B = 2.79%. The main structural parameters of $La_{2.91}Bi_{0.09}BWO_9$ are compiled in Table 1. According to the refinement, we are sure that there is no impurity phase which can afford other site for Bi^{3+} ions to occupy. Figure 1c shows the XRD patterns of LBW:xBi^{3+} samples, along with the simulated standard pattern based on the refined results. All the reflections can be indexed in hexagonal phase of La_3BWO_9 with $P6_3$ space group (no. 173). This result shows that these samples are pure and that Bi^{3+} dopants are exactly incorporated in La_3BWO_9 host without leading to other phase or impurity. At high temperatures, bismuth is unstable and can readily form diverse valence states in different types of host materials. For that reason, the representative samples were checked by XPS with high purity α-Bi_2O_3 (99.999%) as a reference. The Bi 4f spectrum exhibits two contributions, $4f_{5/2}$ and $4f_{7/2}$ (resulting from the spin−orbit splitting), located at 164.6 and 159.6 eV respectively, which can be exactly assigned to α-Bi_2O_3 (Figure 1d).[29,30] The characteristic peaks of Bi^{3+} in LBW:xBi^{3+} (x = 1.0, 2.0, and 3.0%) samples match well with α-Bi_2O_3, indicating that the valence state of Bi is +3 and trivalent Bi^{3+} ions dominate in all the samples.

3.2. Optical Band Gap of La_3BWO_9. The DRS of LBW:xBi^{3+} (x = 0, 0.5, 1.0, 2.0, and 3.0%) samples are shown Figure 2. The broad band at 200−300 nm in the blank

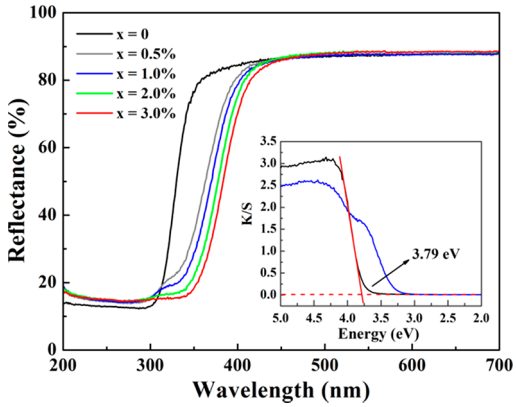

Figure 2. Diffuse reflection spectra of La_3BWO_9:xBi^{3+} samples. The inset shows the absorption spectra of La_3BWO_9 (black line) and La_3BWO_9:1.0%Bi^{3+} (blue line) samples.

sample (x = 0) arises from the intrinsic absorption of La_3BWO_9 host due to the $O^{2-} \rightarrow W^{6+}$ charge transfer transitions. As soon as Bi^{3+} ions are introduced into this compound, a new absorption appears in the 300−400 nm regions, which is attributed to $^1S_0 \rightarrow {}^3P_1$ electronic transitions of Bi^{3+}. The absorption of Bi^{3+} gets enhanced as the doping concentration increases, and the absorption edge shifts from 400 to 450 nm. This is well-matched with the light output of NUV LED chips (λ = 350−410 nm). On the basis of the Kubelka−Munk formula:[31]

$$F(R_\infty) = \frac{(1 - R_\infty)^2}{2R_\infty} = \frac{k}{s} \quad (1)$$

DOI: 10.1021/acsami.8b00808
ACS Appl. Mater. Interfaces 2018, 10, 13660−13668

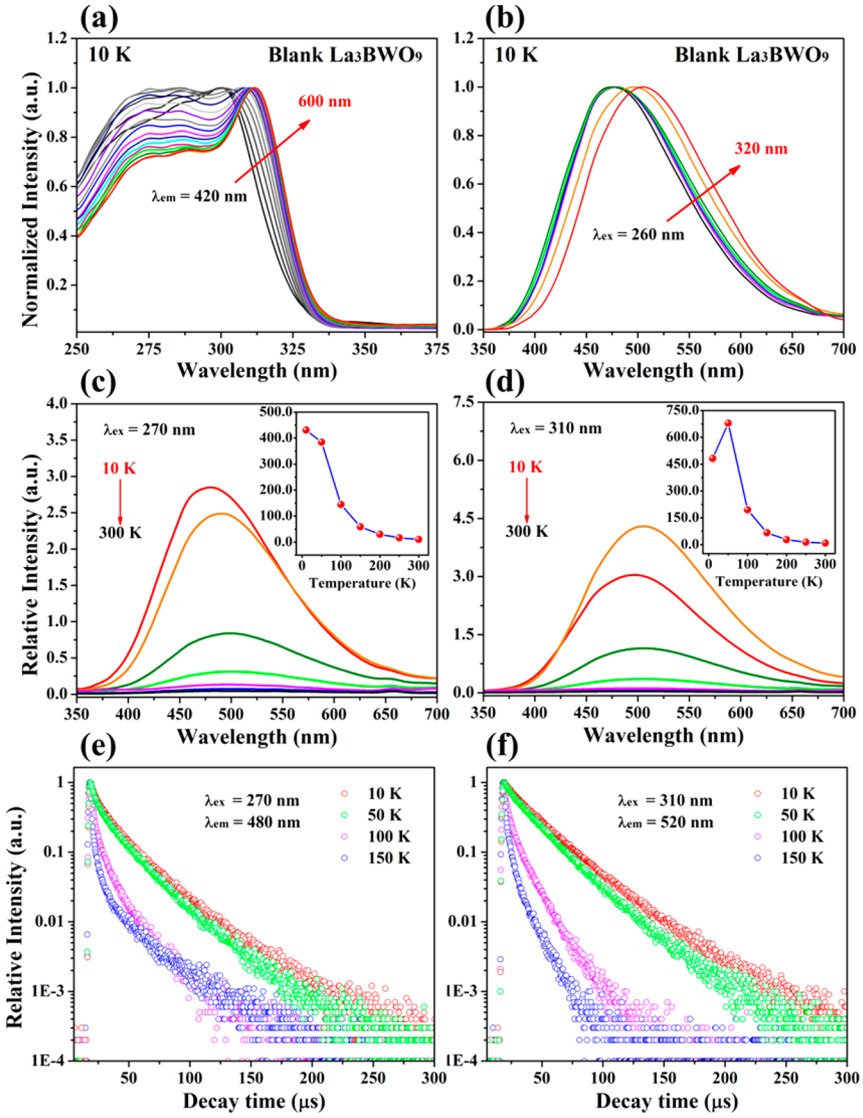

Figure 3. Normalized (a) excitation and (b) emission spectra of blank La_3BWO_9 at 10 K; temperature-dependent emission spectra of blank La_3BWO_9 under the excitation at (c) 270 and (d) 310 nm; inset shows a plot of integrated PL intensity versus temperature; (e and f) decay curves of blank La_3BWO_9 under two different test conditions.

in which R_∞ is the diffuse reflectance of the layer relative to the standard, k is the absorption coefficient, and s is the scattering coefficient. As shown in the inset of Figure 2, the absorption spectra were converted from the DRS. From this plot, the optical band gap (E_g) of La_3BWO_9 compound is ~3.79 eV.

3.3. Photoluminescence Properties. *3.3.1. Luminescent Properties of Blank La_3BWO_9.* Tungstates have been widely studied as a conventional matrix for self-activated luminescent materials owing to their unique WO_4 tetrahedron and WO_6 octahedron groups. In the hexagonal La_3BWO_9, W atoms are 6-fold coordinated by O atoms that form into isolated WO_6 octahedra (see Figure 1a).[28] For octahedral WO_6 group, the electrons from the ground state $^1A_{1g}$ are excited into the $^1T_{1u}$ levels. This excitation process is an allowed electric-dipole transition. Meanwhile, the emitting $^3T_{1u} \rightarrow {}^1A_{1g}$ transition is allowed, the others forbidden.[32] The luminescent properties of La_3BWO_9 were investigated to understand the host contribution to the sample doped with Bi^{3+}. At 10 K, La_3BWO_9 host exhibits a broad absorption band at 250−350 nm, which belongs to the $O^{2-} \rightarrow W^{6+}$ charge transfer band (CTB) originating from $^1A_{1g} \rightarrow {}^1T_{1u}$ transitions of WO_6 groups. Upon the excitation of UV light, the host shows a blue-greenish emission which is attributed to $^3T_{1u} \rightarrow {}^1A_{1g}$ transitions of WO_6 groups. As Figure 3a shows, the excitation peak moves from 270 to 312 nm by tailoring the monitored emission wavelength from 420 to 600 nm. At the same time, the emission peak redshifts from 474 to 504 nm with the increasing of excitation wavelength (260−320 nm), as depicted in Figure 3b. The emission band seems to consist of at least two largely overlapping contributions. However, the PL behavior of tungstate group is very complicated. Because it is common in self-activated compounds, the luminescence from the perturbed WO_6 units is not excluded. This may account for the observed redshift of the excitation and emission peak when the monitored emission and excitation wavelengths are changed, respectively.

Figures 3c and d show the temperature dependence of PL intensity for La_3BWO_9 host under the excitations at 270 and 310 nm, respectively. Each inset presents a plot of integrated intensity versus temperature. As temperature increases to 300 K

DOI: 10.1021/acsami.8b00808
ACS Appl. Mater. Interfaces 2018, 10, 13660−13668

from 10 K, the intensity of the host emission decreases gradually until it disappears completely under 270 nm excitation. By contrast, as excited at 310 nm, the intensity of the host emission first increases and then decreases until it disappears completely, indicating the effective energy transfer among the perturbed WO_6 groups. It is reported that the emitting $^3T_{1u}$ levels can be split into A_{1u}, E_u, T_{1u}, and T_{2u} levels as a result of spin−orbit coupling. One of the latter levels may work as an optical trap to quench the host luminescence.[32]

The decay behaviors of La_3BWO_9 host under two different test conditions are depicted in Figures 3e and f, respectively. The decay curves present a double exponential decay behavior, and the lifetime can be determined by the equation below:[33,34]

$$I = A_1 \exp\left(\frac{-t}{\tau_1}\right) + A_2 \exp\left(\frac{-t}{\tau_2}\right) \quad (2)$$

$$\tau = \frac{A_1\tau_1^2 + A_2\tau_2^2}{A_1\tau_1 + A_2\tau_2} \quad (3)$$

in which I is the PL intensity, τ is the average decay time, A_1 and A_2 are constants, t is the time, and τ_1 and τ_2 are rapid and slow lifetimes for exponential components, respectively. The calculated values of the lifetimes are listed in Table 2. In the two cases, the decay lifetimes are greatly shortened as temperature is raised, which further confirms the quenching of the host luminescence. The decay profiles deviate from single exponential decay rule even at 10 K. At this temperature, the self-trapped excitons that are formed subsequently to the excitation of WO_6 units cannot migrate within the host lattice so that the radiative recombination reaches maximum. Some luminescence killers may, however, occur by energy transfer to nearby sinks. As temperature increases, migration may occur and reach more distant sinks, thus reinforcing the quenching of luminescence. A drastic change of the decay profile was observed between 50 and 100 K, along with the shortening of the decay time. This reveals a second nonradiative path, likely a crossover of the excited state to the ground state. Such very efficient quenching process almost totally kills the host luminescence at RT. As a result, the PL of the host at RT is so weak that it can be ignored and will be no longer discussed in what follows.

Table 2. Decay Lifetimes (τ) of La_3BWO_9 Host in the Two Different Cases

	τ_{ave} (μs)	
temperature (K)	λ_{ex} = 270 nm, λ_{em} = 480 nm	λ_{ex} = 310 nm, λ_{em} = 520 nm
10	20.39	27.67
50	18.82	23.94
100	5.10	8.59
150	4.13	3.04

3.3.2. Luminescent Properties of LBW:Bi^{3+} Phosphors. Figure 4 describes the excitation and emission spectra of LBW:Bi^{3+} phosphors at RT. The doping of Bi^{3+} results in a broadband yellow emission centered at ∼560 nm, as shown in Figure 4a. Since the intrinsic host luminescence is quenched at RT, this new emission is attributed undoubtedly to $^3P_1 \rightarrow {}^1S_0$ transitions of Bi^{3+}. As excited at 340 nm, emission intensity of Bi^{3+} increases gradually with an increasing Bi^{3+} content, and then it decreases when Bi^{3+} content x exceeds 1.5% on account of the concentration quenching effect. The normalized

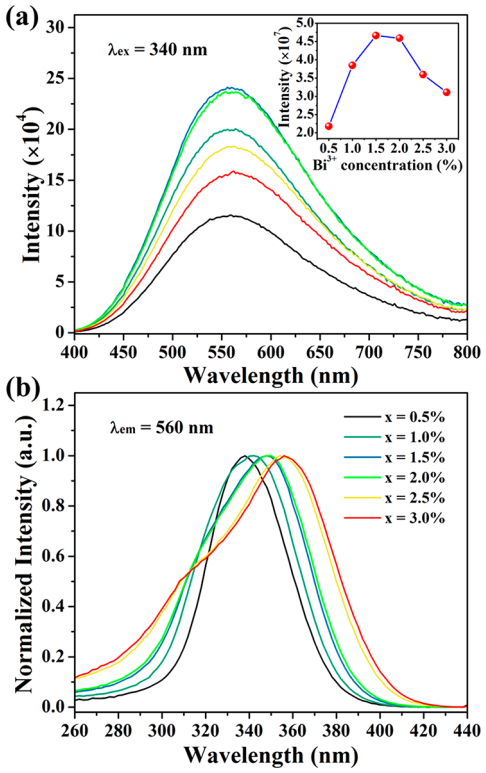

Figure 4. (a) Photoluminescence spectra and (b) photoluminescence excitation spectra of La_3BWO_9:xBi^{3+} phosphors at room temperature; inset shows the integrated PL intensity as a function of Bi^{3+} concentration.

excitation spectra monitored at 560 nm are displayed in Figure 4b. These samples have strong excitation in NUV arising from $^1S_0 \rightarrow {}^3P_1$ transitions of Bi^{3+}, which is consistent with DRS spectra (see Figure 2). With the increases in Bi^{3+} content, the excitation peak shifts from 326 to 350 nm, revealing that there exist more than one Bi^{3+}luminescent center in LBW:Bi^{3+} phosphor. We notice the absence of the host-related excitation, meaning the inefficient host sensitization to Bi^{3+} luminescence in this material. So, the quantum efficiency of LBW:1.5%Bi^{3+} is poor, and only 19.2% under the excitation at 370 nm. We believe that it can be further improved by optimizing the synthetic conditions.

To clarify the PL behavior of Bi^{3+}, the PLE and PL spectra of LBW:1.5%Bi^{3+} phosphor at RT were investigated in detail. As Figure 5a shows, the excitation peak moves from 326 to 350 nm as the monitored emission wavelength increases from 450 to 600 nm. Accordingly, the emission peak suffers from a redshift from 540 to 580 nm when the excitation wavelength varies from 250 to 380 nm, as displayed in Figure 5b. This emission consists of two overlapping bands at ∼540 and ∼580 nm, whose relative intensity strongly relies on the excitation wavelength; the longer the excitation wavelength, the more the contribution of the latter band. On the basis of these results, we can conclude that there are two Bi^{3+} luminescent centers in the host lattice. To have deeper insight, the PLE and PL spectra were converted to an energy scale and deconvoluted into two Gaussian profiles, which are derived from two independent La sites occupied by Bi^{3+} ions corresponding to Bi(I) and Bi(II), respectively. The fitted excitation and emission bands of Bi(I) and Bi(II) are plotted in Figures 5c and d, and the

DOI: 10.1021/acsami.8b00808
ACS Appl. Mater. Interfaces 2018, 10, 13660−13668

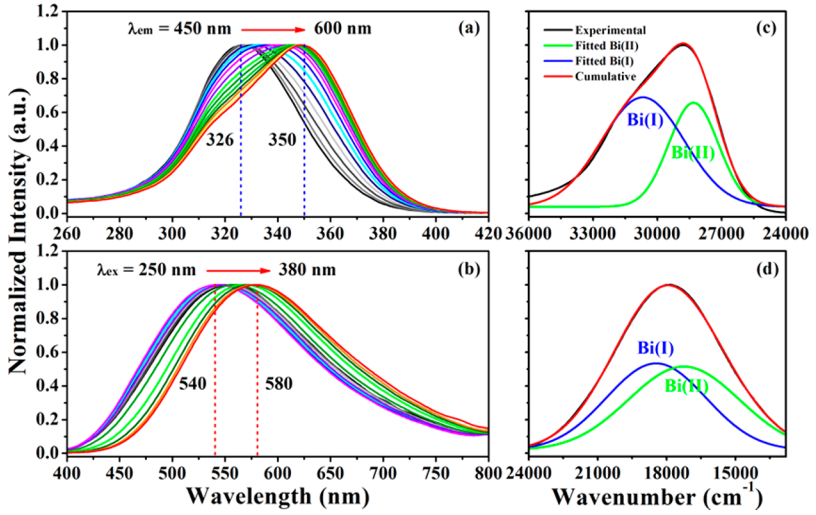

Figure 5. Normalized (a) excitation and (b) emission spectra of La_3BWO_9:1.5%Bi^{3+} phosphor at room temperature; the fitted (c) excitation and (d) emission bands of Bi(I) and Bi(II) by Gaussian deconvolution.

corresponding goodness of fittings are 99.45 and 99.97%, respectively.

Generally, the decay lifetimes of activator ions at distinct crystallographic sites should differ from each other.[35,36] The decay curves of Bi(I) and Bi(II) emission are depicted in Figures 6a and b, respectively. The decay behaviors are

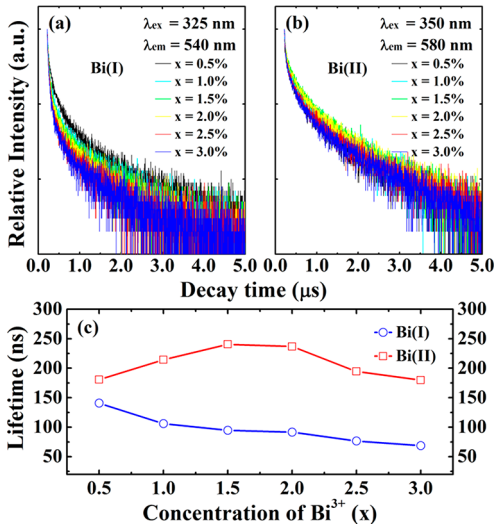

Figure 6. Decay curves of (a) Bi(I) and (b) Bi (II) luminescent centers in La_3BWO_9:xBi^{3+} phosphors; (c) decay lifetimes of Bi(I) and Bi (II) as a function of Bi^{3+} concentration.

nonexponential and difficult to interpret with accuracy owing to the large spectral overlap between Bi(I) and Bi(II). For this reason, only average lifetimes can be calculated with[37,38]

$$\tau = \frac{\int tI(t)\mathrm{d}t}{\int I(t)\mathrm{d}t} \quad (4)$$

in which $I(t)$ represents the PL intensity at time t. The values of τ are summarized in Table 3. With the continuous introducing of Bi^{3+}, the decay time of Bi(I) gradually decreases from 140.72 to 68.69 ns (see Figure 6c). In contrast, the decay curves of Bi(II) show a difference. The decay time increases initially and

Table 3. Decay Lifetimes (τ) of Bi(I) and Bi(II) in La_3BWO_9:xBi^{3+} Phosphors

	τ_{ave} (ns)	
x (mol %)	Bi(I)	Bi(II)
0.5	140.72	180.73
1.0	105.83	214.25
1.5	94.71	240.57
2.0	91.46	236.70
2.5	76.62	194.41
3.0	68.69	179.64

decreases afterward (see Figure 6c), indicating an effective energy transfer from Bi(I) to Bi(II). The decay behaviors further support the conclusion of existing double Bi^{3+} luminescent centers in LBW:Bi^{3+} phosphor.

3.3.3. GBW:Bi^{3+} vs LBW:Bi^{3+}. Gd_3BWO_9 used to be considered isostructural with La_3BWO_9, and it crystallizes in a hexagonal crystal system with $P6_3$ space group (no. 173).[26] Only one Gd site in the structure can accept Bi^{3+} ions. It follows that Gd_3BWO_9:Bi^{3+} (GBW:Bi^{3+}) should have identical or similar luminescent property with LBW:Bi^{3+} if they were really isostructural. The normalized excitation and emission spectra of GBW:Bi^{3+} were used as a reference for comparison with LBW:Bi^{3+}, as illustrated in Figure 7. The test conditions were kept same for both samples. As Figure 7a shows, the excitation peak of GBW:Bi^{3+} stays the same as the monitored emission wavelength changes; the emission peak of GBW:Bi^{3+} remains almost unchanged as the excitation wavelength increases (see Figure 7b). By contrast, the excitation peak of LBW:Bi^{3+} redshifts from 326 to 350 nm (see Figure 5a); the emission peak of LBW:Bi^{3+} suffers from a large redshift from 540 to 580 nm, as displayed in Figure 5b. This phenomenon means that there is only one Bi^{3+} luminescent center in GBW:Bi^{3+} phosphor but two Bi^{3+} luminescent centers in LBW:Bi^{3+} phosphor. The PL behavior of Bi^{3+} in GBW:Bi^{3+} phosphor agrees with the hexagonal structure of Gd_3BWO_9, but that in LBW:Bi^{3+} phosphor cannot consist with the established crystal structure of La_3BWO_9. Therefore, it is certain that La_3BWO_9 must differ from Gd_3BWO_9 and crystallize in a different space group.

DOI: 10.1021/acsami.8b00808
ACS Appl. Mater. Interfaces 2018, 10, 13660−13668

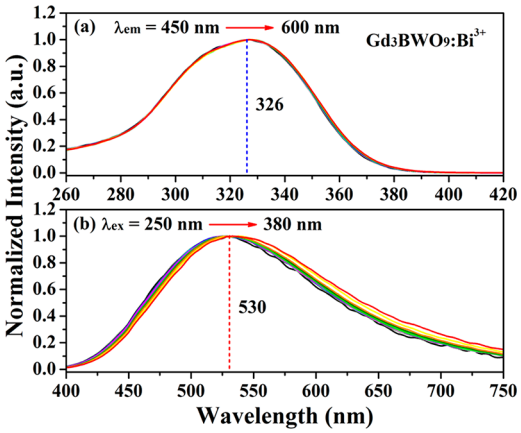

Figure 7. (a) Photoluminescence excitation and (b) photoluminescence spectra of $Gd_3BWO_9:Bi^{3+}$ phosphor as a reference for comparison with $La_3BWO_9:Bi^{3+}$ phosphor.

3.4. Redefinition of Crystal Structure for La_3BWO_9.

Photoluminescence has been regarded as an effective way to verify the controversial crystal structure because of its high sensitivity to crystallographic sites. Taking what has been mentioned above into account, we conclude that La_3BWO_9 crystallizes in another crystal structure in which two independent crystallographic La sites survive. In this case, we should choose a more reasonable space group rather than $P6_3$ for La_3BWO_9. Looking up all of Ln_3BWO_9 compounds, we found that only Eu_3BWO_9 is unique trigonal structure with $P3$ space group in which there are two different crystallographic Eu sites.[28] Rietveld refinements were implemented to redefine the crystal structure of La_3BWO_9. The crystallographic data of Eu_3BWO_9 were used as an initial model. There are two La sites in this model, and the occupancy of both of them by Bi^{3+} ions is consistent with the observed experimental phenomena. So, we decided to occupy all La sites by Bi^{3+} ions, but the values were fixed to 0.03 due to the complex model and their unstable refinement. In the process of Rietveld refinement, two La sites can offer the great capacity to accept Bi^{3+} ions, and the temperature factors for atoms in these La sites were constrained to the same. Figure 8a shows the observed, calculated, and difference results of the XRD refinement for $La_{2.91}Bi_{0.09}BWO_9$. The final reliability factors are converged to R_{wp} = 7.72% and R_B = 2.59%, which are lower than those refined in the $P6_3$ space group (R_{wp} = 8.05%, R_B = 2.79%). The final refined structural parameters for $La_{2.91}Bi_{0.09}BWO_9$ are listed in Table 4. In the trigonal structure of La_3BWO_9, La atoms are coordinated with eight and nine O atoms to form irregular polyhedra $La1O_8$ and $La2O_9$ sharing edges with octahedral WO_6 groups, as depicted in Figure 8b. The additional XRD data of $La_3BWO_9:xBi^{3+}$ (x = 0, 0.5, 1.0, 1.5, 2.0, and 2.5%) were measured in the 2θ range from 10 to 80° with an interval of 0.02°. Profile fitting was performed using Le Bail method. The dependence of the cell parameters on Bi^{3+} content is plotted in Figure 9. The cell volume V appears an increasing trend as Bi^{3+} content increases. This implies the successful substitution of the larger Bi^{3+} ions (CN = 8, IR = 1.17 Å) for the smaller La^{3+} ions (CN = 8, IR = 1.16 Å).

The emission peak position strongly depends on the crystal field splitting of activator, in particular for Eu^{2+}, Ce^{3+}, and Bi^{3+}. The crystal field splitting (Δ) can be expressed with the equation as follows:[39,40]

$$\Delta = \frac{Ze^2r^4}{6R^5} \quad (5)$$

in which Δ is a measure of the energy level separation, Z is the anion charge, e is the electron charge, r is the radius of the d wave function, and R is the bond length. An inspection of the trigonal structure of La_3BWO_9 shows that the average bond length of La1−O is shorter than that of La2−O. According to eq 5, the covalency and crystal field effect for the La1 site are larger than those for the La2 site. Hence, the lower-energy Bi(II) emission is ascribed to the La1 site and the higher-energy Bi(I) emission to the La2 site.

The microstructure and morphology of LBW:Bi^{3+} sample were observed by electron microscope technique. The (0001) plane was caught in $La_{2.91}Bi_{0.09}BWO_9$ sample by the SAED pattern shown in Figure 10a. This is a strong evidence for $P3$ space group because the reflection (0001) is absent in $P6_3$ space group according to the extinction rule: reflections with (000l), l = 2n + 1, must have zero intensity; only reflections with (000l), l = 2n, have nonzero intensity. The existence of (0001) peak further confirms that the real space group is $P3$. The sharp spots and the absence of any diffuse streaks indicate the good crystallization and rule out the existence of any stacking defects. Moreover, we observed that the particles of LBW:1.5%Bi^{3+} phosphor are uniformly smooth, as shown in Figure 10b.

4. CONCLUSION

In summary, we synthesized a series of LBW:Bi^{3+} phosphors by traditional solid state reaction. LBW:Bi^{3+} possess strong excitation in NUV region, and their yellow emission spans

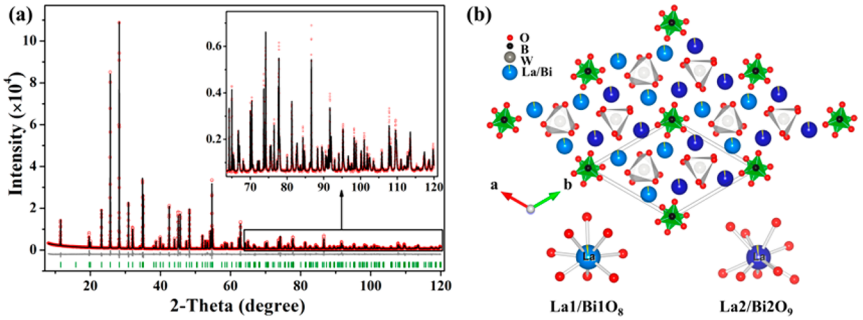

Figure 8. (a) Observed (red dots) and calculated (black solid line) XRD patterns as well as difference profile (gray solid line) of Rietveld refinement for $La_{2.91}Bi_{0.09}BWO_9$ in $P3$ space group; the green ticks mark the Bragg reflection positions. (b) Trigonal structure of $La_{2.91}Bi_{0.09}BWO_9$ and La/Bi-centered polyhedra.

DOI: 10.1021/acsami.8b00808
ACS Appl. Mater. Interfaces 2018, 10, 13660−13668

Table 4. Refined Structural Parameters for $La_{2.91}Bi_{0.09}BWO_9$ in *P*3 Space Group

atom	site	*x*	*y*	*z*	occ.	B_{iso} (Å^2)
W1	1b	1/3	2/3	1/4	1	0.7(3)
W2	1a	2/3	1/3	0.770 (2)	1	0.4(3)
La1	3d	0.363(1)	0.084(1)	0.229(2)	0.97	0.5(2)
Bi1	3d	0.363(1)	0.084(1)	0.229(2)	0.03	0.5(2)
La2	3d	0.278(1)	0.365(1)	0.737(1)	0.97	1.0(2)
Bi2	3d	0.278(1)	0.365(1)	0.737(1)	0.03	1.0(2)
B1	1c	0	0	0.36(3)	1	2(1)
B2	1c	0	0	0.84(3)	1	2(1)
O1	3d	0.172(4)	0.056(4)	0.839(5)	1	1.5(3)
O2	3d	0.138(5)	0.169(5)	0.418(6)	1	1.5(3)
O3	3d	0.181(5)	0.498(4)	−0.017(7)	1	1.5(3)
O4	3d	0.728(4)	0.198(4)	0.594(5)	1	1.5(3)
O5	3d	0.134(5)	0.502(5)	0.427(6)	1	1.5(3)
O6	3d	0.617(5)	0.143(5)	−0.004(7)	1	1.5(3)
cell parameters	a = 8.84326 (5) Å, c = 5.57553 (4) Å, V = 377.608 (5) Å^3					
R factors	R_P = 5.37%, R_{wp} = 7.72%, R_B = 2.59%, χ^2 = 2.81					

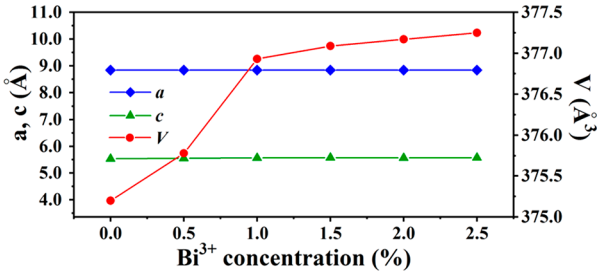

Figure 9. Cell parameters *a*, *c*, and *V* as a function of Bi^{3+} concentration (*x*) in La_3BWO_9:*x*Bi^{3+} samples.

from 400 to 800 nm peaked at 560 nm. XPS analysis proves that the dominant valence state of Bi is +3. The PL spectroscopy analysis indicates that there are two Bi^{3+} luminescent centers in LBW:Bi^{3+} phosphor, which is in contradiction with the previously reported hexagonal structure of La_3BWO_9 with $P6_3$ space group because of only one La site in this structure. Combining the PL properties of Bi^{3+} with Rietveld refinement, La_3BWO_9 was redefined as a trigonal crystal structure with lower space group *P*3 in which there are two independent crystallographic La sites. This result is in agreement with the observed experimental result of two luminescent centers of Bi^{3+}. In addition, the rationalization of *P*3 space group was further confirmed by the finding of the reflection (0001) based on the extinction rule. This work is expected to provide a new insight into evaluating the crystal structure for a given host compound by luminescent probe of Bi^{3+} ions.

AUTHOR INFORMATION

Corresponding Author

*E-mail: pengmingying@scut.edu.cn; Tel: +86-(0)20-22236910; Fax: +86-(0)20-87114204.

ORCID

Jin Han: 0000-0002-0062-0352
Maxim S. Molokeev: 0000-0002-8297-0945
Mingying Peng: 0000-0002-0053-2774
Jing Wang: 0000-0002-1246-991X

Notes

The authors declare no competing financial interest.

ACKNOWLEDGMENTS

This work was financially supported by the National Natural Science Foundation of China (Grant 51672085), the Key Program of Guangzhou Scientific Research Special Project (Grant 201607020009), the Program for Innovative Research Team in University of Ministry of Education of China (Grant IRT_17R38), and the National Key Research and Development Plan (Grant 2017YFF0104504).

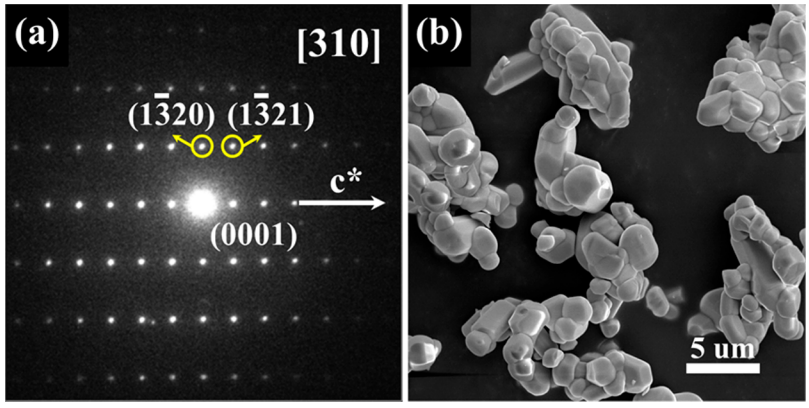

Figure 10. (a) SAED pattern taken along the [310] zone axis of $La_{2.91}Bi_{0.09}BWO_9$ sample; (b) SEM image of La_3BWO_9:1.5%Bi^{3+} sample.

DOI: 10.1021/acsami.8b00808
ACS Appl. Mater. Interfaces 2018, 10, 13660−13668

REFERENCES

(1) Schubert, E. F.; Kim, J. K. Solid-State Light Sources Getting Smart. *Science* **2005**, *308*, 1274−1278.
(2) Schubert, E. F.; Kim, J. K.; Luo, H.; Xi, J.-Q. Solid-State Lighting—A Benevolent Technology. *Rep. Prog. Phys.* **2006**, *69*, 3069−3099.
(3) Pimputkar, S.; Speck, J. S.; DenBaars, S. P.; Nakamura, S. Prospects for LED Lighting. *Nat. Photonics* **2009**, *3*, 180−182.
(4) Pust, P.; Schmidt, P. J.; Schnick, W. A Revolution in Lighting. *Nat. Mater.* **2015**, *14*, 454−458.
(5) Feldmann, C.; Jüstel, T.; Ronda, C. R.; Schmidt, P. J. Inorganic Luminescent Materials: 100 Years of Research and Application. *Adv. Funct. Mater.* **2003**, *13*, 511−516.
(6) Ye, S.; Xiao, F.; Pan, Y. X.; Ma, Y. Y.; Zhang, Q. Y. Phosphors in Phosphor-Converted White Light-Emitting Diodes: Recent Advances in Materials, Techniques and Properties. *Mater. Sci. Eng., R* **2010**, *71*, 1−34.
(7) Lin, C. C.; Liu, R. S. Advances in Phosphors for Light-Emitting Diodes. *J. Phys. Chem. Lett.* **2011**, *2*, 1268−1277.
(8) Xia, Z. G.; Liu, Q. L. Progress in Discovery and Structural Design of Color Conversion Phosphors for LEDs. *Prog. Mater. Sci.* **2016**, *84*, 59−117.
(9) Lin, C. C.; Meijerink, A.; Liu, R. S. Critical Red Components for Next-Generation White LEDs. *J. Phys. Chem. Lett.* **2016**, *7*, 495−503.
(10) Huang, X. Y. Solid-State Lighting: Red Phosphor Converts White LEDs. *Nat. Photonics* **2014**, *8*, 748−749.
(11) Li, J. H.; Yan, J.; Wen, D. W.; Khan, W. U.; Shi, J. X.; Wu, M. M.; Su, Q.; Tanner, P. A. Advanced Red Phosphors for White Light-Emitting Diodes. *J. Mater. Chem. C* **2016**, *4*, 8611−8623.
(12) Li, G. G.; Tian, Y.; Zhao, Y.; Lin, J. Recent Progress in Luminescence Tuning of Ce^{3+} and Eu^{2+}-Activated Phosphors for pc-WLEDs. *Chem. Soc. Rev.* **2015**, *44*, 8688−8713.
(13) Park, J. K.; Kim, C. H.; Park, S. H.; Park, H. D.; Choi, S. Y. Application of Strontium Silicate Yellow Phosphor for White Light-Emitting Diodes. *Appl. Phys. Lett.* **2004**, *84*, 1647−1649.
(14) Saradhi, M. P.; Varadaraju, U. V. Photoluminescence Studies on Eu^{2+}-Activated Li_2SrSiO_4—A Potential Orange-Yellow Phosphor for Solid-State Lighting. *Chem. Mater.* **2006**, *18*, 5267−5272.
(15) Huang, C. H.; Chiu, Y. C.; Yeh, Y. T.; Chan, T. S.; Chen, T. M. Eu^{2+}-Activated $Sr_8ZnSc(PO_4)_7$: A Novel near-Ultraviolet Converting Yellow-Emitting Phosphor for White Light-Emitting Diodes. *ACS Appl. Mater. Interfaces* **2012**, *4*, 6661−6668.
(16) Zhang, L. L.; Zhang, J. H.; Zhang, X.; Hao, Z. D.; Zhao, H. F.; Luo, Y. S. New Yellow-Emitting Nitride Phosphor $SrAlSi_4N_7:Ce^{3+}$ and Important Role of Excessive AlN in Material Synthesis. *ACS Appl. Mater. Interfaces* **2013**, *5*, 12839−12846.
(17) Durach, D.; Neudert, L.; Schmidt, P. J.; Oeckler, O.; Schnick, W. $La_3BaSi_5N_9O_2:Ce^{3+}$ − A Yellow Phosphor with an Unprecedented Tetrahedra Network Structure Investigated by Combination of Electron Microscopy and Synchrotron X-Ray Diffraction. *Chem. Mater.* **2015**, *27*, 4832−4838.
(18) Blasse, G.; Bril, A. Investigations on Bi^{3+}-Activated Phosphors. *J. Chem. Phys.* **1968**, *48*, 217−222.
(19) Boutinaud, P. Revisiting the Spectroscopy of the Bi^{3+} Ion in Oxide Compounds. *Inorg. Chem.* **2013**, *52*, 6028−6038.
(20) Han, J.; Li, L. J.; Peng, M. Y.; Huang, B. L.; Pan, F. J.; Kang, F. W.; Li, L. Y.; Wang, J.; Lei, B. F. Toward Bi^{3+} Red Luminescence with No Visible Reabsorption through Manageable Energy Interaction and Crystal Defect Modulation in Single Bi^{3+}-Doped $ZnWO_4$ Crystal. *Chem. Mater.* **2017**, *29*, 8412−8424.
(21) Kang, F. W.; Peng, M. Y.; Lei, D. Y.; Zhang, Q. Y. Recoverable and Unrecoverable Bi^{3+}-Related Photoemissions Induced by Thermal Expansion and Contraction in $LuVO_4:Bi^{3+}$ and $ScVO_4:Bi^{3+}$ Compounds. *Chem. Mater.* **2016**, *28*, 7807−7815.
(22) Zhu, R.; Huang, Y.; Seo, H. J. A Red-Emitting Phosphor of Eu-Based Borotungstate Eu_3BWO_9 for White Light-Emitting Diodes. *J. Electrochem. Soc.* **2010**, *157*, H1116−H1120.
(23) Liu, J. Y.; Wang, J.; Zhang, Z. J.; Chen, H. H.; Yang, X. X.; Li, R. F.; Zhao, J. T. Photoluminescence Properties of Red-Emitting Phosphors $Ln_3BWO_9:Eu^{3+}$ (Ln = Y, La, Gd). *J. Lumin.* **2012**, *132*, 2874−2878.
(24) Huang, J. P.; Hou, B. H.; Ling, H. Y.; Liu, J.; Yu, X. B. Crystal Structure, Electronic Structure, and Photoluminescence Properties of $La_3BW_{1-x}Mo_xO_9:Eu^{3+}$ Red Phosphor. *Inorg. Chem.* **2014**, *53*, 9541−9547.
(25) Mączka, M.; Tomaszewski, P.; Stępień-Damm, J.; Majchrowski, A.; Macalik, L.; Hanuza, J. Crystal Structure and Vibrational Properties of Nonlinear Eu_3BWO_9 and Nd_3BWO_9 Crystals. *J. Solid State Chem.* **2004**, *177*, 3595−3602.
(26) Krut'ko, V. A.; Belik, A. A.; Lysanova, G. V. Structures of Nonlinear Hexagonal Boratotungstates Ln_3BWO_9 (Ln = La, Pr, Nd, Sm, Gd, Tb, Dy). *Russ. J. Inorg. Chem.* **2006**, *51*, 884−889.
(27) Coelho, A. A. *TOPAS Academic*, version 4.1; Coelho Software: Brisbane, Australia, 2007.
(28) Gokhman, L.; Dzhurinskij, B.; Efremov, V.; Ilyukhin, A.; Chistova, V. Synthesis and Structure of Boratotungstates Ln_3BWO_9 (Ln = La, Pr, Nd, Sm-Ho). *Russ. J. Inorg. Chem.* **1994**, *39*, 1026−1030.
(29) Kang, F. W.; Zhang, H. S.; Wondraczek, L.; Yang, X. B.; Zhang, Y.; Lei, D. Y.; Peng, M. Y. Band-Gap Modulation in Single Bi^{3+}-Doped Yttrium−Scandium−Niobium Vanadates for Color Tuning over the Whole Visible Spectrum. *Chem. Mater.* **2016**, *28*, 2692−2703.
(30) Zhang, K.; Ma, C. G.; Zhang, J. Y.; Liu, B. M.; Zhou, Y.; Guo, S. Q.; Xu, J. Y.; Hou, J. S.; Fang, Y. Z.; Zheng, L. R.; Sun, H. T. Giant Enhancement of Luminescence from Phosphors through Oxygen-Vacancy-Mediated Chemical Pressure Relaxation. *Adv. Opt. Mater.* **2017**, *5*, 1700448.
(31) Tandon, S. P.; Gupta, J. P. Measurement of Forbidden Energy Gap of Semiconductors by Diffuse Reflectance Technique. *Phys. Status Solidi B* **1970**, *38*, 363−367.
(32) Blasse, G. The Luminescence of Closed-Shell Transition-Metal Complexes. New Developments. In *Luminescence and Energy Transfer*; Springer Berlin Heidelberg: Berlin, Heidelberg, 1980; pp 1−41.
(33) Li, M. Q.; Zhang, J. L.; Han, J.; Qiu, Z. X.; Zhou, W. L.; Yu, L. P.; Li, Z. Q.; Lian, S. X. Changing Ce^{3+} Content and Codoping Mn^{2+} Induced Tunable Emission and Energy Transfer in $Ca_{2.5}Sr_{0.5}Al_2O_6:Ce^{3+},Mn^{2+}$. *Inorg. Chem.* **2017**, *56*, 241−251.
(34) Xu, H. B.; Zhuang, W. D.; Wang, L.; Liu, R. H.; Liu, Y. H.; Liu, L. H.; Cho, Y.; Hirosaki, N.; Xie, R. J. Synthesis and Photoluminescence Properties of a Blue-Emitting $La_3Si_8N_{11}O_4:Eu^{2+}$ Phosphor. *Inorg. Chem.* **2017**, *56*, 14170−14177.
(35) Zhou, W. J.; Pan, F. J.; Zhou, L.; Hou, D. J.; Huang, Y.; Tao, Y.; Liang, H. B. Site Occupancies, Luminescence, and Thermometric Properties of $LiY_9(SiO_4)_6O_2:Ce^{3+}$ Phosphors. *Inorg. Chem.* **2016**, *55*, 10415−10424.
(36) Zhang, X. J.; Wang, J.; Huang, L.; Pan, F. J.; Chen, Y.; Lei, B. F.; Peng, M. Y.; Wu, M. M. Tunable Luminescent Properties and Concentration-Dependent, Site-Preferable Distribution of Eu^{2+} Ions in Silicate Glass for White LEDs Applications. *ACS Appl. Mater. Interfaces* **2015**, *7*, 10044−10054.
(37) Jiao, M. M.; Jia, Y. C.; Lu, W.; Lv, W. Z.; Zhao, Q.; Shao, B. Q.; You, H. P. A Single-Phase White-Emitting $Ca_2SrAl_2O_6:Ce^{3+},Li^+,Mn^{2+}$ Phosphor with Energy Transfer for UV-Excited WLEDs. *Dalton Trans.* **2014**, *43*, 3202−3209.
(38) Wang, B.; Lin, H.; Xu, J.; Chen, H.; Wang, Y. S. $CaMg_2Al_{16}O_{27}:Mn^{4+}$-Based Red Phosphor: A Potential Color Converter for High-Powered Warm W-LED. *ACS Appl. Mater. Interfaces* **2014**, *6*, 22905−22913.
(39) Huang, C. H.; Wu, P. J.; Lee, J. F.; Chen, T. M. $(Ca,Mg,Sr)_9Y(PO_4)_7:Eu^{2+},Mn^{2+}$: Phosphors for White-Light Near-UV LEDs through Crystal Field Tuning and Energy Transfer. *J. Mater. Chem.* **2011**, *21*, 10489−10495.
(40) Chen, M. Y.; Xia, Z. G.; Molokeev, M. S.; Wang, T.; Liu, Q. L. Tuning of Photoluminescence and Local Structures of Substituted Cations in $xSr_2Ca(PO_4)_2−(1-x)Ca_{10}Li(PO_4)_7:Eu^{2+}$ Phosphors. *Chem. Mater.* **2017**, *29*, 1430−1438.

DOI: 10.1021/acsami.8b00808
ACS Appl. Mater. Interfaces 2018, 10, 13660−13668